

## Three-Dimensional Shape-Persistent Fluorescent Nanocages: Facile Dynamic Synthesis, Photophysical Properties, and Surface Morphologies

Jia Luo, Ting Lei, Xiaoguang Xu, Fang-Mei Li, Yuguo Ma,\* Kai Wu,\* and Jian Pei\*<sup>[a]</sup>

Functional nanostructures with intriguing topology and special properties have played important roles in self-assembly, host–guest chemistry, catalysis and nanotechnology.<sup>[1]</sup> Among these nanosized units, shape-persistent artificial architectures provide fixed conformations, which might offer many advantages for predictable assembly, nanofabrication, or guest inclusion.<sup>[1,2]</sup> Recently, many rigid cages with confined cavities through multivalent assembly have attracted considerable interest due to their applications in delivery, extraction, detection and various microreactors.<sup>[1a,c,3]</sup> However, the synthesis of shape-persistent molecules is usually laborious, and the structural diversification in different dimensions from a common parent is also difficult; on the other hand, rational design of molecules with desired functionalities still remains a great challenge. Therefore, it is imperative to develop a well-organized structure to meet the requirement of readily available diversification and rational design of derivatives with controllable solubility and processibility, which also provides the possibility to agilely mimic multivalent assembly in nature.<sup>[4]</sup>

In our previous contribution, we reported a unique 3D skeleton **4a** as shown in Scheme 1 for pure blue emitters applied in organic light-emitting diodes.<sup>[5]</sup> The success of synthesizing such skeleton provides us with convenience to realize the structural diversity of 3D derivatives through orthogonally and distinguishably modifiable sites. As a result, such a 3D structure would offer various derivatives with diverse functionalities. Herein, we utilize this 3D functionalized “body” (a covalent template) to couple with suitable planar “caps” to achieve quantitative formation of  $C_3$  symmetrical nanocages **1a–c** with intensive visible luminescence through

dynamic covalent chemistry (DCC). DCC emerges as an efficient and versatile synthetic strategy due to its “error-checking” and “proof-reading” features, generating thermodynamically controlled products by virtue of its reversibility.<sup>[6]</sup> Additionally, the selective introduction of three conjugated arms not only guarantees the fluorescent property, but also offers the interactions between host and guest.

Scheme 2 illustrates the synthetic route to nanocages **1a–c** and their reduced forms  $H_{12}$ -**1a–c**. First, demethylation of 3D skeleton **4a** by  $BBr_3$  followed by reacting with *n*-hexylbromide or 2-(2-(2-methoxyethoxy)ethoxy)ethyl 4-methylbenzenesulfonate (TEG-OTs) under basic condition afforded **4b** or **4c** in high yield. Subsequently, efficient Pd-catalyzed Suzuki cross-coupling reaction between **4** and 4-formylphenylboronic ester gave desired aldehyde **2** in good yields (75–86%). Compared with weak noncovalent interactions such as hydrogen-bonding and metal–ligand coordination, imine condensation between aldehydes and amines seems to be the most valid choice to construct more stable nanocages.<sup>[6c]</sup> First, the formation of the nanocages from aldehyde **2a** and two equivalents of amine **3**<sup>[7]</sup> was carried out in refluxing  $CHCl_3$  or  $CH_2Cl_2$  solution. However, amounts of precipitates were formed and  $^1H$  NMR spectra of the in situ mixture suggested that an undesirable mixture was formed even after extended heating time, which might be owing to the poor solubility of the imine intermediates and starting materials in  $CHCl_3$  or  $CH_2Cl_2$ . 1,1,2,2-Tetrachloroethane (TCE) was employed as a co-solvent to promote the condensation reaction. To our delight, refluxing the mixture



Scheme 1. Structures and structural schematic diagram of three-dimensional skeletons.

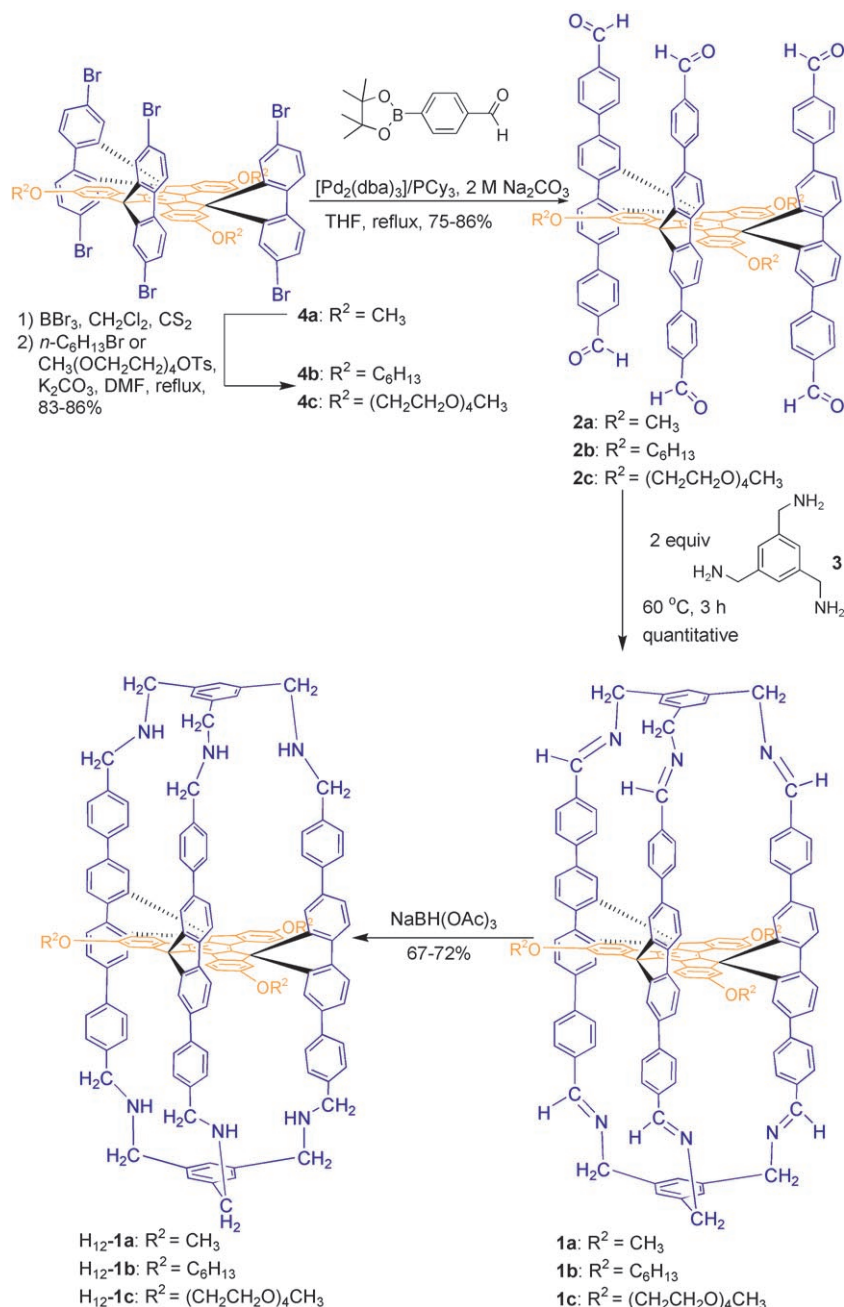
[a] J. Luo, T. Lei, X. Xu, F.-M. Li, Prof. Y. Ma, Prof. K. Wu, Prof. J. Pei Key Laboratories of Bioorganic Chemistry and Molecular Engineering and of Polymer Chemistry and Physics of Ministry of Education, College of Chemistry Peking University, Beijing 100871 (PR China)  
Fax: (+86) 10-62758145  
E-mail: jianpei@pku.edu.cn

Supporting information for this article is available on the WWW under <http://www.chemistry.org> or from the author.

for 3 h resulted in a homogeneous solution, in which nanocage **1a** was quantitatively constructed, as evidenced by  $^1\text{H}$  NMR spectroscopy. After removal of the solvents under reduced pressure, nanocage **1a** was obtained as a slightly yellow solid without further purification.

Figure 1 compares the partial  $^1\text{H}$  NMR spectra (300 MHz,  $\text{CDCl}_3$ , 298 K) of **2a**, **3** and nanocage **1a**. Compared with that of **2a** in Figure 1a, the signal assigned to CHO ( $\delta = 9.91$  ppm) in the  $^1\text{H}$  NMR spectrum of **1a** (Figure 1c) disappeared, and a new signal ( $\delta = 7.69$  ppm) assigned to imine protons emerged, which shifted upfield (about 0.44 ppm) relative to that of the corresponding proton in normal imine groups.<sup>[8]</sup> Furthermore, after the transformation from amine **3** to imine **1a**, the signals of  $\text{CH}_2$  showed downfield shift from  $\delta = 3.88$  ppm (singlet in Figure 1b) to 4.94 ppm (dd in Figure 1c), which was due to geminal coupling ( $J = 15.6$  Hz) caused by the unsymmetrical chemical environment in our rigid nanocage. Moreover, its chemical shift moved downfield (about 0.26 ppm) in comparison with those of the corresponding imines within an open scaffold.<sup>[8]</sup> MALDI-TOF MS analysis of **1a**, as shown in Figure 2, further confirmed the proposed cage structure and the quantitative formation: only an ion peak at  $m/z = 1729.8$  for  $[\text{M} + \text{H}]^+$  (calcd for  $\text{C}_{126}\text{H}_{84}\text{N}_6\text{O}_3$ : 1728.7) was observed, and the isotopic distribution fit well with the theoretically predicted pattern. All the characterization data verified the formation and the purity of cage **1a**.

Figure 3 illustrates the  $^1\text{H}$  NMR spectra of the mixture (**2a/3** 1:2) in  $\text{CDCl}_3/\text{C}_2\text{D}_2\text{Cl}_4$  1:1 at 333 K as time elapsed. A signal of formyl protons at chemical shift 9.98 ppm appeared and finally all signals of formyl protons disappeared as time went by. These results indicated that the system was gradually transformed to imine, and eventually became the symmetrical species after formation of many unsymmetrical intermediates. After 40 min, the signal at about  $\delta = 5.00$  ppm



Scheme 2. Synthetic route to fluorescent cages **1a**, **1b**, and **1c**, and their reductive cages  $\text{H}_{12}\text{-1a}$ ,  $\text{H}_{12}\text{-1b}$ , and  $\text{H}_{12}\text{-1c}$ .

emerged, concomitant with decrease of the singlet signal at  $\delta = 3.88$  ppm. The transformation became complete in about 130 min. Obviously, the clean  $^1\text{H}$  NMR spectra indicate that there are no oligomers or polymers in the final products. As the  $^1\text{H}$  NMR spectra show, there are only two signals emerged at about 10 ppm, which means only two kinds of formyl protons could be observed in  $^1\text{H}$  NMR spectra. Thus, we proposed that the formation of the imine bonds contained a self-accelerating process. After one arm of a cap was connected to the “main body”, the reaction rates for the formation of the other two imine bonds became much

faster, so the only intermediate observed through  $^1\text{H NMR}$  was one-end capped structure, although its structure need to be further elucidated. Apparently, such a phenomenon can be attributed to the multivalent effect directed by our rigid structure, which accelerated the reaction rates in contrast with previous reports.<sup>[4b]</sup>

Nanocages **1b** and **1c** from **2b** or **2c** were also formed quantitatively in refluxing  $\text{CHCl}_3$  solution. Due to the introduction of *n*-hexyl and TEG chains, the solubility of such skeletons in common organic solvents was significantly improved. We also observed that the solubility of the intermediates and products turned out to be crucial in the thermodynamically controlled process. Nanocages **1b** and **1c** also exhibited the similar  $^1\text{H NMR}$  and mass spectroscopic behaviors (See the Supporting Information). In addition, the cage formation reactions were carried out quantitatively without any added acid catalysis. All the above data show that the desired nanocages are thermodynamically stable products irrespective of substituted "tails" in planar truxene moiety. Although the imine bonds were reversible, our desired nanocages were stable both in solution and solid state.

To completely "fix" our cages, reduction of **2** by  $\text{NaBH}(\text{OAc})_3$  was carried out and the  $^1\text{H NMR}$  and MALDI-TOF MS spectra indicated that all the six imine bonds were reduced to saturated amines. As shown in Figure 1d, the resonance signals of  $\text{CH}_2$  ( $\text{H}_k$ ) in the "cap" were shifted upfield by about 1.05 ppm, resulting from the imine transformation. In consideration of the decrease of rigidity after the reduction, the split resonance signal of  $\text{H}_k$  tended to merge. In addition, a new singlet peak emerged at  $\delta=3.59$  ppm which was as-

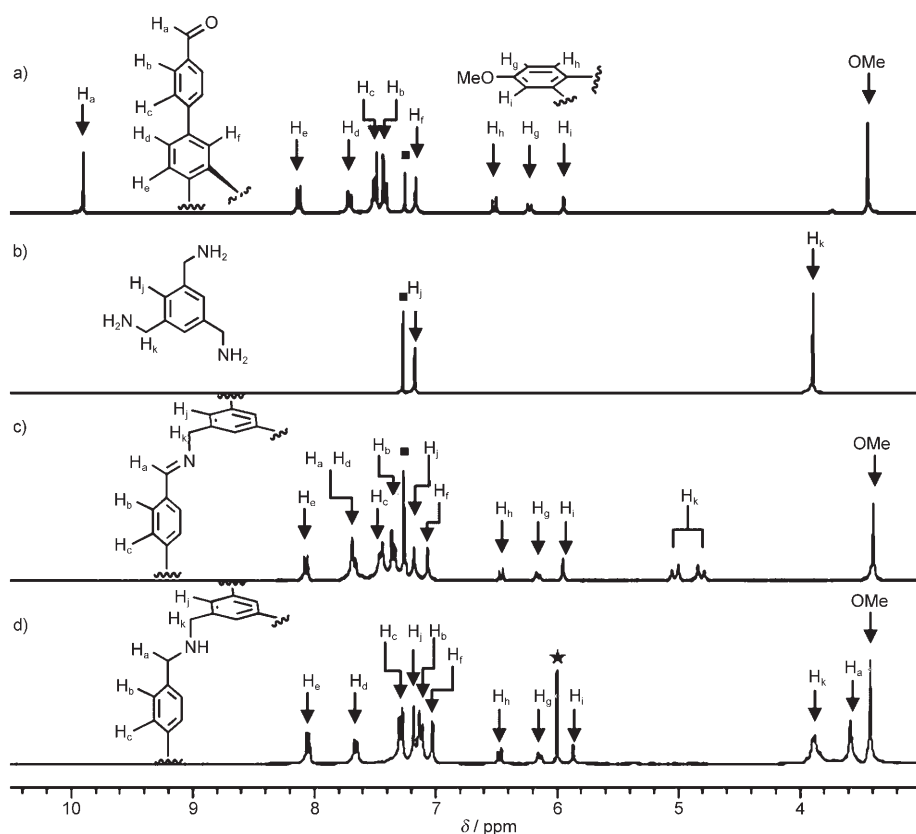


Figure 1. Partial  $^1\text{H NMR}$  ( $\text{CDCl}_3$ , 300 MHz, 298 K) spectra of a) **2a**, b) **3**, c) **1a** produced in situ, and  $^1\text{H NMR}$  ( $\text{C}_2\text{D}_2\text{Cl}_4$ , 300 MHz, 298 K) spectra of d)  $\text{H}_{12}$ -**1a**. ■ and ★ denote  $\text{CDCl}_3$  and  $\text{C}_2\text{D}_2\text{Cl}_4$ , respectively.

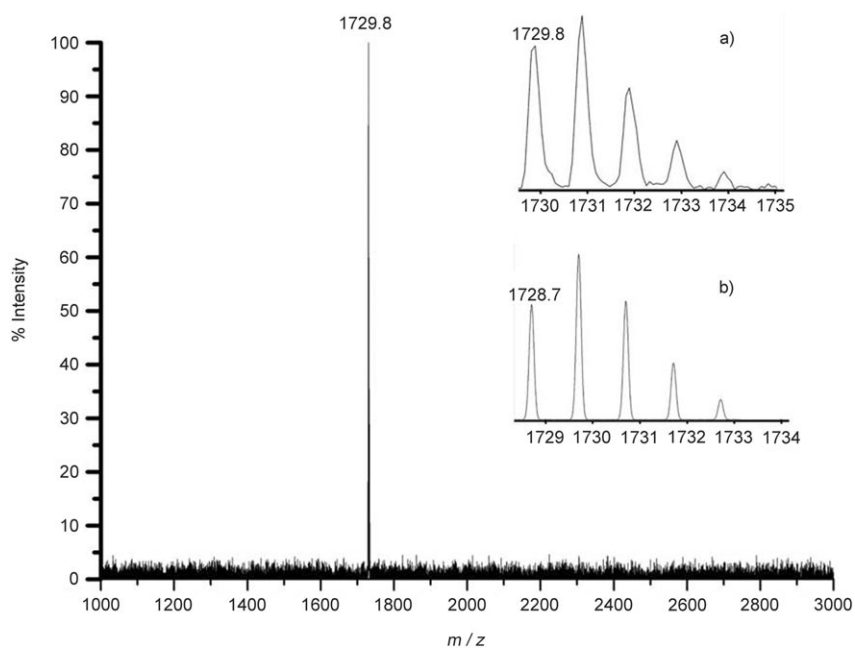


Figure 2. MALDI-TOF MS spectrum of nanocage **1a**. Insets a) and b) are corresponding to experimental and theoretical isotopic distributions, respectively.

signed to the signal of  $\text{CH}_2$  converted from  $\text{CH}=\text{N}$ . MALDI-TOF MS analysis of  $\text{H}_{12}$ -**1a** further confirmed the formation

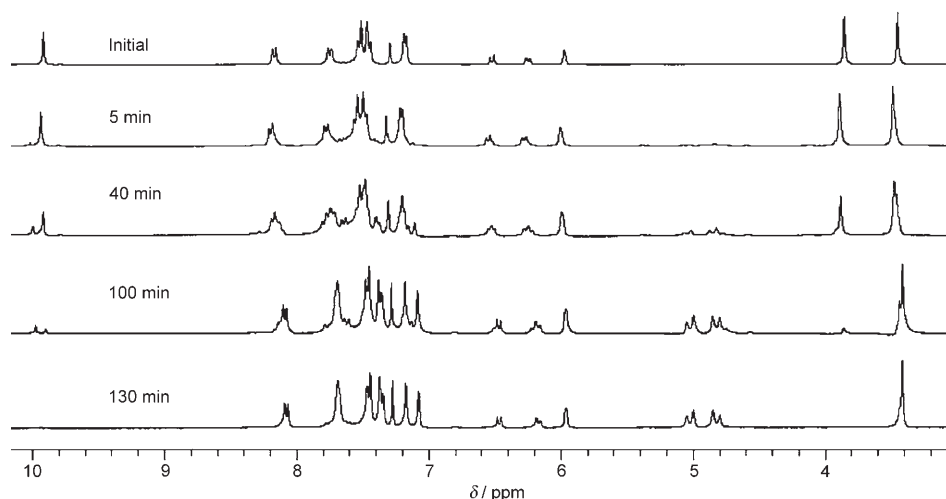


Figure 3. Partial  $^1\text{H}$  NMR spectra ( $\text{CDCl}_3/\text{C}_2\text{D}_2\text{Cl}_4$  1:1) of the **2a** and **3** (6.6 mM/13.2 mM) mixture at 333 K as a function of time.

of the proposed reductive cage: only one ion peak at  $m/z = 1741.6$  for  $[\text{M}+\text{H}]^+$  (calcd for  $\text{C}_{126}\text{H}_{96}\text{N}_6\text{O}_3$ : 1740.8) was observed.

The photophysical properties of nanocages **1a–c** and their corresponding reduced forms  $\text{H}_{12}$ -**1a–c** were first investigated in dilute solution. Figure 4 shows the absorption and photoluminescent (PL) spectra of **2a**, **1a**, and  $\text{H}_{12}$ -**1a** in dilute  $\text{C}_2\text{H}_2\text{Cl}_4$  solution. Compounds **2a** and **1a** showed an identical absorption peak at 323 nm, being assigned to the 2,2',7,7'-tetraphenyl-9,9'-spirobifluorene fragment.<sup>[9]</sup> Moreover, in their absorption spectra, both **2a** and **1a** exhibited a shoulder at about 348 nm. This registers the similarity in the effective conjugation length between aldehyde **2a** and nanocage **1a**. However, the onset of the absorption spectrum of **2a** red-shifted from 410 nm to about 470 nm, and the absorption intensity of the shoulder feature decreased. After reduction,  $\text{H}_{12}$ -**1a** showed an absorption peak at 322 nm with two shoulders at 310 and 300 nm. In dilute  $\text{C}_2\text{H}_2\text{Cl}_4$  solution, the PL spectrum of **2a** showed a peak at 450 nm. The PL maximum  $\lambda_{\text{max}}$  of **1a** slightly red-shifted about 8 nm in comparison with that of **2a**. The reductive cage  $\text{H}_{12}$ -**1a** emitted blue light with a wavelength of 396 nm in  $\text{C}_2\text{H}_2\text{Cl}_4$  solution. Other cages **1b** and **1c** also showed similar absorption and PL spectra. Both **2** and **1** emitted sharp greenish-blue color under the UV light irradiation.

The surface morphologies of these nanocages **1a–c** were also investigated.<sup>[3h]</sup> According to molecular modeling, the height of cage **1a** is about 1.5 nm. The highly dilute  $\text{C}_2\text{H}_2\text{Cl}_4$  solution of nanocage **1a** ( $3.0 \times 10^{-6}$  M) was drop-cast onto the mica substrate and the surface pattern was analyzed by tapping-mode atomic force microscopy (TM-AFM). The TM-AFM experiments and section analysis showed the presence of monodisperse entities protruding from the surface of the mica substrate, as shown in Figure 5a. Sectional analysis revealed that these entities had a height of  $1.37 \pm 0.14$  nm (average of 30 measurements), in consistence with the height of nanocage **1a**. This result suggested that the nano-

cage molecules were distributed on the mica surface, and they stood. However, when  $\text{CHCl}_3$  solution ( $3.0 \times 10^{-6}$  M) of nanocage **1b** was drop-cast onto the mica surface, the TM-AFM experiments and sectional analysis showed the presence of many clusters with larger size on the substrate, and the surface morphologies were very different from those of nanocage **1a** shown in Figure 5b. The height of these clusters were measured to be in the range of 0.9–1.6 nm (average of 30 measurements) by sectional analysis. This implied that the van der Waals in-

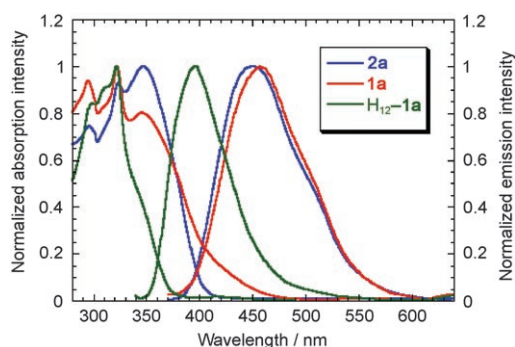


Figure 4. UV/Vis absorption and PL spectra of **2a**, nanocages **1a**,  $\text{H}_{12}$ -**1a** in dilute  $\text{C}_2\text{H}_2\text{Cl}_4$  solution ( $c = 1.0 \times 10^{-6}$  M). Emission spectra were recorded upon excitation at absorption maximum.

teraction between *n*-hexyloxy chains led to larger aggregation and non-uniform height fluctuation upon evaporation of the solvent. Interestingly, once the  $\text{R}^2$  substituents were swapped to the polar TEG groups, the surface pattern changed: after the drop-casting of **1c** ( $3.0 \times 10^{-6}$  M in  $\text{CHCl}_3$ ) onto the mica surface, the nanocages formed uniformed morphologies, both horizontally and vertically, in Figure 5c. Sectional analysis revealed that these uniform entities had a height of  $0.91 \pm 0.07$  nm (average of 30 measurements). Because of the incapability of imaging in detail the flexible TEG chains with AFM, we speculate that such a height might be associated with the nanocages with their TEG chains stretched over the polar mica surface, possibly due to the strong interaction between polar TEG chains and hydrophilic mica substrate. Figure 5d shows the structural schematic diagram of nanocages **1a–c**. Figure 5a–c also illustrate the schematic representations of the surface morphologies of nanocages **1a–c** on the mica substrate.

In summary, we have developed a facile approach to synthesizing a series of 3D shape-persistent fluorescent nanocages by applying the concept of dynamic covalent chemis-

try. Time-dependent  $^1\text{H}$  NMR analyses indicate that multivalent bonds of these nanocages between aldehydes and amines can be facily and effectively constructed in situ. This process is quantitative, and shape-persistent artificial nanocage structures are selectively formed as the most thermodynamically stable species in the reaction mixture. More interestingly, our 3D skeleton provides double cavities in one molecule through double capping, showing the possibility to integrate two different guests into one molecule. These *dynamic* cages are trapped to become *fixed* ones by  $\text{NaBH}(\text{OAc})_3$  in moderate yields. Moreover, variations of the flexible substitution groups in the planar moiety hardly affect the conformations of the nanocages; these substituting groups not only adjust the solubility of the nanocages, but also dramatically change the aggregation behaviors and the surface morphologies. Systematic investigation of their photophysical properties shows that all cages give off visible light from blue to greenish-blue in dilute  $\text{C}_2\text{H}_2\text{Cl}_4$  solutions. Applications of these attracting properties in sensors and probes are ongoing in our lab. All in all, these results demonstrate that the utilization of such skeletons for 3D nanostructure assembly opens a new pathway to exploit the mechanical bond at the molecular level in chemistry.

### Acknowledgements

This work was financially supported by the Major State Basic Research Development Program (Nos. 2006CB921602 and 2007CB808000) and by the National Natural Science Foundation of China (NSFC, 20632020, 50673002, 20425207). Mr. Jia Luo thanks the Peking University CDY scholarship for generous support.

**Keywords:** atomic force microscopy • cage compounds • host-guest systems • nanostructures • NMR spectroscopy

[1] a) S. R. Seidel, P. J. Stang, *Acc. Chem. Res.* **2002**, *35*, 972–983; b) S. Höger, *Chem. Eur. J.* **2004**, *10*, 1320–1329; c) M. Fujita, M. Tomimaga, A. Hori, B. Therrien, *Acc. Chem. Res.* **2005**, *38*, 371–380; d) W. Zhang, J. S. Moore, *Angew. Chem.* **2006**, *118*, 4524–4548; *Angew. Chem. Int. Ed.* **2006**, *45*, 4416–4439.

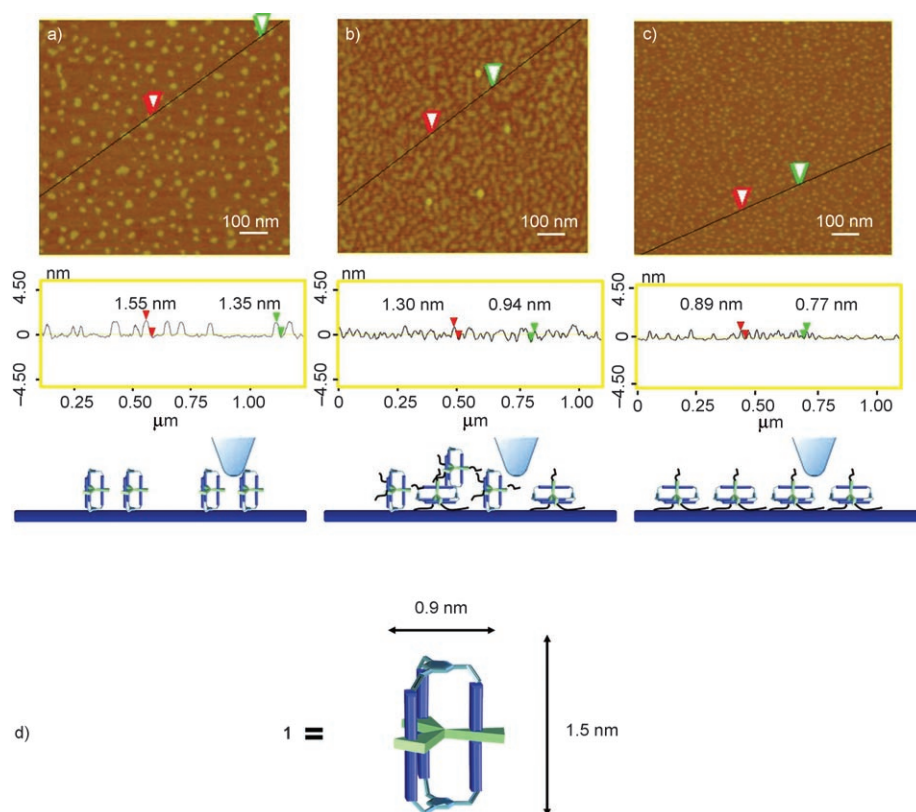


Figure 5. Tapping-Mode AFM height images ( $1\ \mu\text{m} \times 1\ \mu\text{m}$ ), sectional analyses and schematic representations of the surface assembling morphologies of a) **1a**, b) **1b** and c) **1c** on mica substrate, and d) structural schematic diagram of **1** with its flexible chains  $\text{R}^2$  omitted. Calculated volume of each cavity is about  $120\ \text{\AA}^3$  (optimized by MMFF94).

- [2] a) T. Heinz, D. M. Rudkevich, J. Rebek, Jr., *Nature* **1998**, *394*, 764–766; b) G. W. Orr, L. J. Barbour, J. L. Atwood, *Science* **1999**, *285*, 1049–1051; c) J. L. Atwood, L. J. Barbour, A. Jerga, *Science* **2002**, *296*, 2367–2369; d) J. L. Atwood, L. J. Barbour, A. Jerga, B. L. Schotter, *Science* **2002**, *298*, 1000–1002; e) M. Yoshizawa, M. Tamura, M. Fujita, *J. Am. Chem. Soc.* **2004**, *126*, 6846–6847; f) A. Lützen, *Angew. Chem.* **2005**, *117*, 1022–1025; *Angew. Chem. Int. Ed.* **2005**, *44*, 1000–1002; g) S. J. Dalgarno, S. A. Tucker, D. B. Bassil, J. L. Atwood, *Science* **2005**, *309*, 2037–2039; h) M. Yoshizawa, M. Tamura, M. Fujita, *Science* **2006**, *312*, 251–254; i) G. V. Oshovsky, D. N. Reinhoudt, W. Verboom, *Angew. Chem.* **2007**, *119*, 2418–2445; *Angew. Chem. Int. Ed.* **2007**, *46*, 2366–2393; j) M. D. Pluth, R. G. Bergman, K. N. Raymond, *Science* **2007**, *316*, 85–88; k) C. Schmuck, *Angew. Chem.* **2007**, *119*, 5932–5935; *Angew. Chem. Int. Ed.* **2007**, *46*, 5830–5833; l) R. J. Hooley, H. J. van Anda, J. Rebek, Jr., *J. Am. Chem. Soc.* **2007**, *129*, 13464–13473.
- [3] For cage-like molecules formed via hydrogen bonding, see a) C. T. Seto, G. M. Whitesides, *J. Am. Chem. Soc.* **1993**, *115*, 905–916; b) A. Arduini, L. Domiano, L. Oglisio, A. Pochini, A. Secchi, R. Ungaro, *J. Org. Chem.* **1997**, *62*, 7866–7868; c) T. Martin, U. Obst, J. Rebek, Jr., *Science* **1998**, *281*, 1842–1845; d) T. Heinz, D. M. Rudkevich, J. Rebek, Jr., *Nature* **1998**, *394*, 764–766; e) T. Grawe, T. Schrader, R. Zadnarm, A. Kraft, *J. Org. Chem.* **2002**, *67*, 3755–3763; f) J. M. C. A. Kerckhoffs, F. W. B. van Leeuwen, A. L. Spek, H. Kooijman, M. Crego-Calama, D. N. Reinhoudt, *Angew. Chem.* **2003**, *115*, 5895–5900; *Angew. Chem. Int. Ed.* **2003**, *42*, 5717–5722; for cage-like molecules formed via metal coordination, see g) L. Baldini, P. Ballester, A. Casnati, R. M. Gomila, C. A. Hunter, F. Sansone, R. Ungaro, *J. Am. Chem. Soc.* **2003**, *125*, 14181–14189; h) E. Menozzi, R. Pinalli, E. A. Speets, B. J. Ravoo, E. Dalcanale, D. N. Reinhoudt, *Chem. Eur. J.* **2004**, *10*, 2199–2206; i) R. Pinalli, V. Cristini, V. Sottili, S. Geremia,

- M. Campagnolo, A. Caneschi, E. Dalcanale, *J. Am. Chem. Soc.* **2004**, *126*, 6516–6517; j) S. Sato, J. Iida, K. Suzuki, M. Kawano, T. Ozeki, M. Fujita, *Science* **2006**, *313*, 1273–1276; k) Q.-H. Yuan, L.-J. Wan, H. Jude, P. J. Stang, *J. Am. Chem. Soc.* **2005**, *127*, 16279–16286; l) P. Ballester, A. I. Oliva, A. Costa, P. M. Deya, A. Frontera, R. M. Gomila, C. A. Hunter, *J. Am. Chem. Soc.* **2006**, *128*, 5560–5569; m) M. Yamanaka, Y. Yamada, Y. Sei, K. Yamaguchi, K. Kobayashi, *J. Am. Chem. Soc.* **2006**, *128*, 1531–1539; n) K. Harano, S. Hiraoka, M. Shionoya, *J. Am. Chem. Soc.* **2007**, *129*, 5300–5301.
- [4] a) J. D. Badjic, S. J. Cantrill, R. H. Grubbs, E. N. Guidry, R. Orenes, J. F. Stoddart, *Angew. Chem.* **2004**, *116*, 3335–3340; *Angew. Chem. Int. Ed.* **2004**, *43*, 3273–3278; b) J. D. Badjic, A. Nelson, S. J. Cantrill, W. B. Turnbull, J. F. Stoddart, *Acc. Chem. Res.* **2005**, *38*, 723–732.
- [5] J. Luo, Y. Zhou, Z.-Q. Niu, Q.-F. Zhou, Y. Ma, J. Pei, *J. Am. Chem. Soc.* **2007**, *129*, 11314–11315.
- [6] For dynamic covalent chemistry, see a) S. Ro, S. J. Rowan, A. R. Pease, D. J. Cram, J. F. Stoddart, *Org. Lett.* **2000**, *2*, 2411–2414; b) S. J. Rowan, S. J. Cantrill, G. R. L. Cousins, J. K. M. Sanders, J. F. Stoddart, *Angew. Chem.* **2002**, *114*, 938–993; *Angew. Chem. Int. Ed.* **2002**, *41*, 898–952; c) K. S. Chichak, S. J. Cantrill, A. R. Pease, S.-H. Chiu, G. W. V. Cave, J. L. Atwood, J. F. Stoddart, *Science* **2004**, *304*, 1308–1312; d) K. C.-F. Leung, F. Arico, S. J. Cantrill, J. F. Stoddart, *J. Am. Chem. Soc.* **2005**, *127*, 5808–5810; e) B. H. Northrop, F. Arico, N. Tangchiavang, J. D. Badjic, J. F. Stoddart, *Org. Lett.* **2006**, *8*, 3899–3902; f) X. Liu, R. Warmuth, *J. Am. Chem. Soc.* **2006**, *128*, 14120–14127; g) C. S. Hartley, E. L. Elliott, J. S. Moore, *J. Am. Chem. Soc.* **2007**, *129*, 4512–4513; h) C. S. Hartley, J. S. Moore, *J. Am. Chem. Soc.* **2007**, *129*, 11682–11683.
- [7] T. Grawe, T. Schrader, R. Zadmand, A. Kraft, *J. Org. Chem.* **2002**, *67*, 3755–3763.
- [8] We synthesized compound **6** by reacting **2a** with benzylamine and we found that the chemical shifts of corresponding imine protons ( $H_a$ ) and methylene protons ( $H_k$ ) were 8.13 and 4.68 ppm in this compound, respectively. It indicated that  $H_a$  was shielded by the capping benzene in cage. More details are shown in the Supporting Information.
- [9] J. Salbeck, N. Yu, J. Bauer, F. Weissortel, H. Bestgen, *Synth. Met.* **1997**, *91*, 209–215.

Received: January 25, 2008  
Published online: April 2, 2008